Alignment tensor versus director: Description of defects in nematic liquid crystals

A. Sonnet, A. Kilian, and S. Hess
Institut für Theoretische Physik, Technische Universität Berlin, D-10623 Berlin, Germany
(Received 22 September 1994; revised manuscript received 9 March 1995)

The core structure of nematic defects cannot be represented by the usual director field, but requires the description by the full *alignment tensor*. We have developed an algorithm which solves a dynamic equation for the alignment tensor in three dimensions (3D). This algorithm is applied to a capillary (2D) and to a spherical droplet (3D), both with perpendicular anchoring. We predict symmetry-breaking, temperature-dependent, first-order configuration transitions both for the capillary and for the droplet geometries as results. These results are compared to known solutions obtained with the standard vectorial calculus.

PACS number(s): 61.30.Jf, 64.70.Md

I. INTRODUCTION

The state of alignment of nematic liquid crystals is characterized by the (symmetric traceless) alignment tensor, sometimes referred to as the Q tensor [1]. It can be measured by birefringence. It is a well defined quantity both in the isotropic and nematic phases and can be used to describe pretransitional effects and strong light scattering [1,2] as well as the phase transition isotropic nematic. The alignment tensor has five degrees of freedom, two of which specify the degree of order, the remaining three are the angles needed to specify the principal directions.

In a uniaxial state only one order parameter (Maier-Saupe) and two angles are needed. The more common director description, which suffices in many but certainly not all applications in nematics, can be used when the order parameter is constant.

The core of a defect in nematics cannot be represented by the director field because biaxiality can occur and the magnitude of the order parameter changes. For this reason it is of interest to apply the alignment tensor theory to physical situations which involve defects in the director description.

As a two-dimensional example, the core of an $s = 1/2$ disclination line has been calculated [3] previously ($s = 1/2$ means that the director field rotates by π when the disclination line is compassed on an arbitrary path). Furthermore, a one-dimensional illustrative example for "biaxial escape" has been presented [4]. In this paper, we look for more examples in two and three dimensions. For simplicity, we will consider untwisted nematics only.

At constant temperature, differences between both formalisms can only be expected when the material is strained. Therefore, we examine geometries that enforce defects: a circle (2D) and a sphere (3D). The circle represents a capillary which is homogeneous along its axis, and the sphere represents a droplet. We restrict ourselves to rigid boundary coupling and perpendicular anchoring (homeotropic). The more complicated "planar-free" boundary conditions [5], which would be appropriate for planar surface alignment, are not considered.

This paper proceeds as follows: in Sec. II, the alignment tensor and its connection to the director are reviewed and the numerical algorithm is described. Section III presents the results, and Sec. IV is devoted to the conclusions.

II. DYNAMIC EQUATIONS AND NUMERICAL ALGORITHMS

A. Alignment tensor and director equations

Phenomenologically, the alignment tensor can be introduced as a quantity proportional to the anisotropic (symmetric-traceless) part of the electric permittivity tensor, i.e.,

$$\underline{\epsilon} = \epsilon^{\mathrm{iso}}\,\underline{\delta} + \epsilon^{a}\,\underline{a}. \tag{1}$$

Here ϵ^a is proportional to the difference $\epsilon_{\parallel} - \epsilon_{\perp}$, where $\epsilon_{\parallel}$ and $\epsilon_{\perp}$ are the permittivities parallel and perpendicular to the molecular symmetry axis for a perfectly oriented sample.

Alternatively, in the framework of statistical physics, the alignment tensor can be defined microscopically via the second moment of the orientational distribution function for the figure axis parallel to the unit vector $\mathbf{u}$,

$$\underline{a} := \sqrt{15/2}\,\langle \overleftrightarrow{\mathbf{uu}} \rangle, \tag{2}$$

of effectively uniaxial particles. The symbol $\leftrightarrow$ denotes the symmetric-traceless part of a tensor, e.g., $\overleftrightarrow{\mathbf{uu}} = \mathbf{uu} - \frac{1}{3}\underline{\delta}$, where $\underline{\delta}$ is the unit tensor. The brackets $\langle\,\rangle$ indicate an orientational average.

In experiments, the dielectric permittivity tensor of thermotropic nematics is usually uniaxial. In this case, $\underline{a}$ can be written in terms of a unit vector $\mathbf{n}$ and the scalar order parameter a as

$$\underline{a} = a\sqrt{3/2}\,\overleftrightarrow{\mathbf{nn}}. \tag{3}$$

In this scaling the relation $a^2 = \mathrm{tr}(\underline{a}^2)$ holds and $a =$

$\sqrt{5}\,S$, where $S = \langle P_2(\mathbf{u}\cdot\mathbf{n})\rangle$ is the Maier-Saupe scalar order parameter.

If, for calculations at constant temperature, the scalar order parameter a is further presumed to be constant, the usual *director* calculus is obtained. It should be noted that the uniaxial alignment tensor (3), which is mathematically a projector, reflects the nematic symmetry, i.e., the physical equivalence of $\mathbf{n}$ and $-\mathbf{n}$.

The results presented in this paper are based on the dynamic equation for the alignment tensor [2,6]

$$\tau_a \frac{\partial \underline{a}}{\partial t} - {\xi_0}^2 \Delta \underline{a} + \underline{\Phi}(\underline{a}) = \underline{0}\ , \tag{4}$$

where $\underline{\Phi}$ is the derivative of a generalized dimensionless Landau–De Gennes potential

$$\phi = \frac{1}{2} A(T)\,\mathrm{tr}(\underline{a}^2) - \frac{\sqrt{6}}{3} B\,\mathrm{tr}(\underline{a}^3) + \frac{1}{4} C\,[\mathrm{tr}(\underline{a}^2)]^2. \tag{5}$$

The parameters τ_a and ξ_0 are a phenomenological relaxation time and a correlation length. They are related to the rotational viscosity γ_1 and the Frank coefficient K (one-constant approximation) by

$$\gamma_1 = n k_B T 3 a_{\mathrm{eq}}^2 \tau_a \tag{6}$$

and

$$K = n k_B T 3 a_{\mathrm{eq}}^2 \xi_0^2. \tag{7}$$

In order to get rid of the material specific constants B and C, the transformations

$$\tilde{\underline{a}} := \frac{3C}{2B}\,\underline{a}, \tag{8}$$

$$\tilde{\xi}_0 := \sqrt{9C/2B^2}\,\xi_0 \tag{9}$$

for all lengths, and

$$\tilde{\tau}_a := (9C/2B^2)\tau_a \tag{10}$$

for the time are applied to (5), which leads to

$$\tilde{\underline{\Phi}} = \vartheta\,\tilde{\underline{a}} - 3\sqrt{6}\,\tilde{\underline{a}}^2 + 2\,\mathrm{tr}(\tilde{\underline{a}}^2)\,\tilde{\underline{a}}, \tag{11}$$

where

$$\vartheta = (9C/2B^2)\,A(T) = \left(1 - \frac{T^*}{T}\right)\left(1 - \frac{T^*}{T_c}\right)^{-1} \tag{12}$$

is used as the temperature variable. In these units the clearing point T_c and the pseudocritical temperature T^* correspond to $\vartheta = 1$ and $\vartheta = 0$, respectively. The tildes are dropped for brevity in all subsequent formulas.

The dimensionless free energy density of the liquid crystal is given by

$$\hat{f} = \frac{{\xi_0}^2}{2} \nabla \underline{a} : \nabla \underline{a} + \phi(\underline{a}). \tag{13}$$

The Euler-Lagrange equations of this energy coincide with the stationary form of (4).

B. The numerical algorithm

Since a symmetric traceless tensor of rank 2 has five degrees of freedom, it is useful to represent $\underline{a}$ in an appropriate base. We choose

$$\underline{T}^0 = \frac{1}{\sqrt{6}}\begin{pmatrix} -1 & 0 & 0 \\ 0 & -1 & 0 \\ 0 & 0 & 2 \end{pmatrix},$$

$$\underline{T}^1 = \frac{1}{\sqrt{2}}\begin{pmatrix} 1 & 0 & 0 \\ 0 & -1 & 0 \\ 0 & 0 & 0 \end{pmatrix},$$

$$\underline{T}^2 = \frac{1}{\sqrt{2}}\begin{pmatrix} 0 & 1 & 0 \\ 1 & 0 & 0 \\ 0 & 0 & 0 \end{pmatrix},$$

$$\underline{T}^3 = \frac{1}{\sqrt{2}}\begin{pmatrix} 0 & 0 & 1 \\ 0 & 0 & 0 \\ 1 & 0 & 0 \end{pmatrix},$$

and

$$\underline{T}^4 = \frac{1}{\sqrt{2}}\begin{pmatrix} 0 & 0 & 0 \\ 0 & 0 & 1 \\ 0 & 1 & 0 \end{pmatrix}, \tag{14}$$

and use

$$\underline{a} = \sum_{i=0}^{4} a_i \underline{T}^i. \tag{15}$$

The five coefficients a_i can be calculated using the orthogonality

$$\mathrm{tr}(\underline{T}^i\,\underline{T}^k) = \delta_{ik}. \tag{16}$$

With this representation, Eq. (4) is a system of five coupled equations [7] which we solve numerically on a rectangular grid. The algorithm is described in detail in [8]. Here we give an outline for the time-independent algorithm.

We start with a finite difference approximation to the stationary version of Eq. (4). The Laplacian is replaced by

$$\frac{\partial^2}{\partial x^2}\underline{a}(x,y,z)$$

$$\to \frac{\underline{a}(x+h,y,z) + \underline{a}(x-h,y,z) - 2\underline{a}(x,y,z)}{h^2} \tag{17}$$

and similar rules for the derivatives in the y and z direction.

A simple iterative fixed point algorithm is obtained by defining $\underline{a}^{\mathrm{new}}$ via

$$\left(\frac{\xi_0}{h}\right)^2 \left[\sum_{\mathbf{i}} \underline{a}^{\mathbf{i}} - 6\underline{a}^{\mathrm{new}}\right] = \underline{\Phi}(\underline{a}^{\mathrm{old}}), \tag{18}$$

where the sum is over the nearest neighbors. This algorithm yields convergence only for values of $\xi_0/h \gtrsim 2$,

which is suitable only for small length scales, because it requires the mesh size h of the discretization grid to be of the order of ξ_0, which in turn is on a molecular scale.

In order to achieve convergence for arbitrary ratios of ξ_0/h, we used an algorithm known as the one-step SOR-Newton method [9]. It arises from a prescription of the form

$$\left(\frac{\xi_0}{h}\right)^2 \left[\sum_{\mathbf{i}} \underline{a}^{\mathbf{i}} - 6\underline{a}^{\text{new}}\right] = \underline{\Phi}(\underline{a}^{\text{new}}). \tag{19}$$

In this case the value for $\underline{a}$ at each grid point is obtained by Newton's method. The resulting linear system of order 5 is solved directly by LU decomposition [10] (where L is a lower triangular matrix and U is an upper triangular one). Performing these steps iteratively for the whole grid yields the desired solution. This algorithm is very robust and suitable for any grid size. The price is the computational work which is increased by a factor 3 compared to an explicit method based on (18).

III. RESULTS

A. Visualization and s=1/2 disclination

Since the alignment tensor has five degrees of freedom, a comprehensive presentation is not as straightforward as for a director field. In order to present the results of our computations, we calculated the alignment tensors eigensystem and the norm of the order parameter according to $\|\underline{a}\| = \sqrt{\text{tr}(\underline{a}^2)}$. The alignment tensor is visualized by a rectangular box which is built from the eigensystem of the tensor. The eigenvalues augmented by $\sqrt{2/3}\,\|\underline{a}\|$ to ensure positivity are used as the edge lengths of the box. Thus it is possible to distinguish between uniaxial (two edges have the same length) and biaxial (all three edges are of different length) alignment. This scheme implies that the size of the box reflects the magnitude of the alignment, e.g., an isotropic tensor would be represented by a very small cube. As an aside, the more natural method to visualize the tensor by an ellipsoid instead of a rectangular box turned out to be less instructive because it is hard to distinguish uniaxial ellipsoids from biaxial ones.

As an example of the visualization of various types of alignment tensors by rectangular boxes, Fig. 1 shows the cross section through an $s = 1/2$ disclination line. Schohpol and Sluckin have previously calculated this solution [3]. We have reproduced it in order to visualize it with our above described scheme, because this type of disclination is an essential part of the symmetry-breaking configurations presented below.

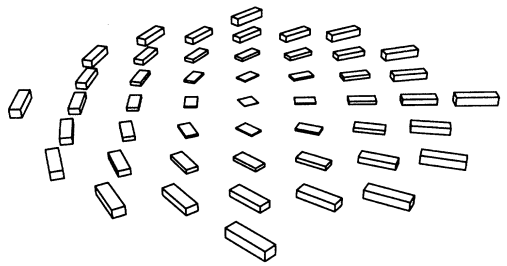

FIG. 1. Core of an s=1/2 disclination. The center is uniaxial with negative Maier-Saupe order parameter (planar uniaxial). It transforms via a biaxial ring into a uniaxial form with a positive S.

The notion of a disclination may be misleading here, because it implies that there may be a defect, i.e., something discontinuous. This, however, holds only if the disclination is described by the director; the alignment tensor always yields a smooth solution. We will nevertheless speak of disclinations, since we refer still to the same physical object.

A typical feature of the $s = 1/2$ disclination is the "biaxial escape," that is the sequence *planar uniaxial* $\leftrightarrow$ *biaxial* $\leftrightarrow$ *uniaxial* with positive S. Note that the 1D example considered in [4] is contained as a special case by the horizontal section through the center.

B. Capillary

We have examined a capillary with fixed perpendicular boundary coupling. This coupling has been realized by uniaxial alignment tensors with their nondegenerate eigenvectors pointing in the direction of the radius and with a magnitude equal to the equilibrium value at the given temperature. Using our tensorial algorithm we have found both solutions with spherical symmetry and with D_2 symmetry. We will use the notations introduced in [11], that is, we will refer to the escaped solution as "escaped-radial" (ER), to the planar and rotationally symmetric solution as "planar-radial" (PR), and to the symmetry-breaking solution as "planar-polar" (PP). The ER solution is uniaxial everywhere, and therefore in this case the more accurate tensorial algorithm yields nothing new. Thus, we will focus on the other solutions, which contain biaxial regions. In Fig. 2, our PR solution is

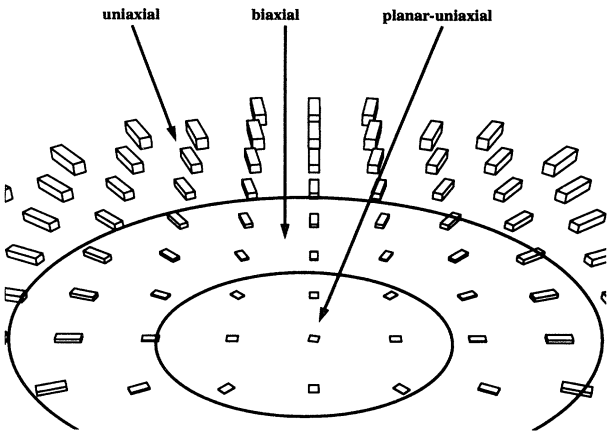

FIG. 2. The rotationally symmetric planar-radial solution, which occurs for very small capillaries close to the nematic isotropic transition temperature. The center is uniaxial with negative Maier-Saupe order parameter S. Via a biaxial ring, the alignment tensor transforms to its usual uniaxial form with positive S.

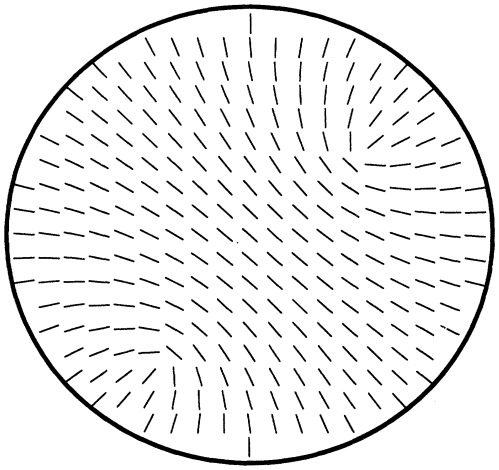

FIG. 3. The symmetry-breaking planar-polar solution that occurs for capillaries larger than those which exhibit the PR configuration. It contains two $s = 1/2$ disclinations which undergo the same biaxial escape as the PR solution.

depicted.

The alignment tensor in the center is uniaxial with a negative Maier-Saupe order parameter (planar uniaxial). It transforms via a biaxial ring into its usual uniaxial form with a positive S (biaxial escape).

We will not present the symmetry-breaking PP solution using the tensor visualization, because the picture would be too complicated and therefore not very elucidating. Instead, we show a solution which we previously obtained using an algorithm which is based on a projector, cf. Eq. (3) [12]. It shows how our solution obtained with the alignment-tensor algorithm in principle looks: in contrast to the PR solution, which is an axial $s = 1$ disclination [1], we have two $s = 1/2$ disclinations. See Fig. 3.

We have calculated a phase diagram that predicts which of the solutions is stable for a given temperature and capillary size. It is shown in Fig. 4. The ER solution,

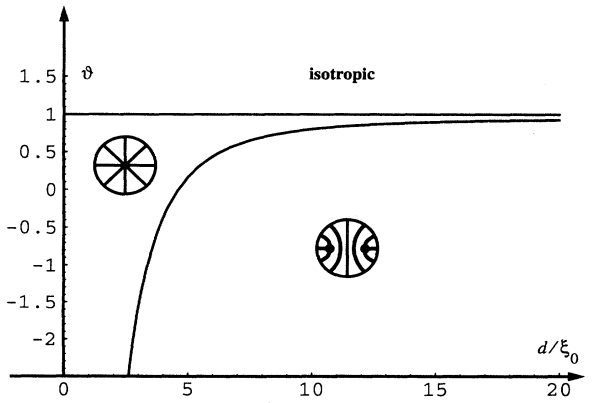

FIG. 4. Phase diagram which predicts the type of solution for a given reduced temperature and reduced capillary size. The depicted solutions are planar-radial (PR), planar-polar (PP), and isotropic.

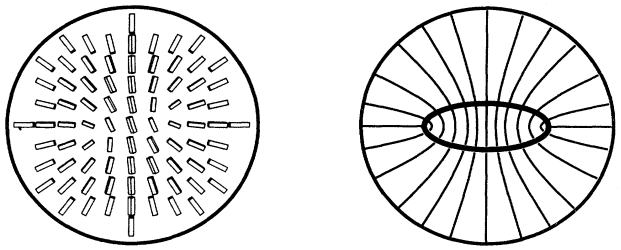

FIG. 5. (a) Symmetry-breaking alignment tensor solution for a homeotropic droplet. Around the center is a small disclination loop. (b) Sketch of the corresponding director field as a supplementary representation.

which is not shown, is minimal for diameters larger than $\approx 40\xi_0$.

C. Droplet

We have examined a droplet with fixed homeotropic boundary coupling, which has been realized in the same way as in the preceding subsection. As a result, we found that the usually assumed spherically symmetric solution should only occur very close to the nematic-isotropic transition temperature, or for very small droplets. In all other cases, a symmetry-breaking solution is energetically preferred. This solution contains an $s = 1/2$ disclination loop around the droplet center. See Fig. 5.

If the droplet is large enough ($d \gtrsim 20\xi_0$), the loop has the diameter $d_{\text{loop}} \approx 10\xi_0$. Figure 6 shows the solution with spherical symmetry. The alignment tensor is zero in a (temperature dependent) center region, and uniaxial elsewhere. The Maier-Saupe order parameter decreases monotonically between the droplet boundary and the center.

Varying the droplet size and the temperature we have found the phase diagram shown in Fig. 7.

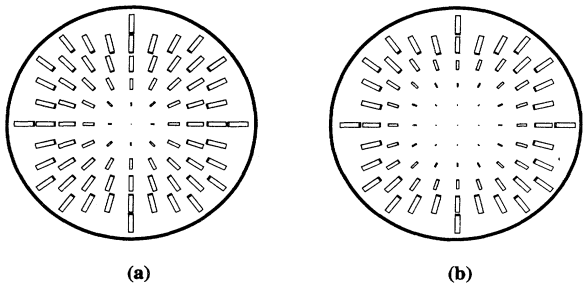

FIG. 6. Spherically symmetric alignment tensor solutions for a homeotropic droplet with $d = 10\xi_0$. The left solution corresponds to the pseudocritical temperature ($\vartheta = 0$), and the right one to the clearing point ($\vartheta = 1$).

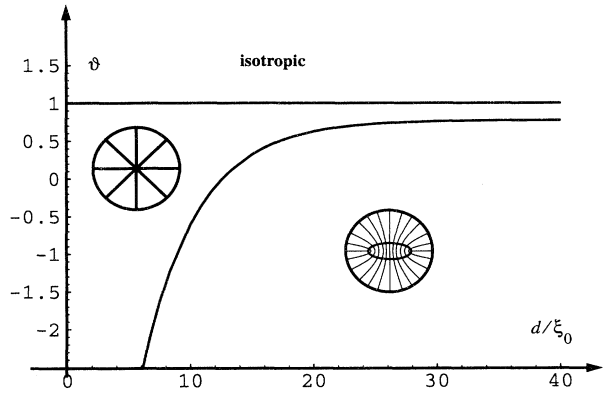

FIG. 7. Phase diagram for the symmetry-breaking configuration transition. The usually assumed spherically symmetric solution occurs only in a very small region of the phase space.

IV. CONCLUSIONS

A. General

The calculations we made are based on a dimensionless and material-independent equation, and are therefore valid for any nematic that can be described by the Landau–De Gennes theory. In order to relate the results to experiments, a material must be specified. We choose *N*-(4′-methoxybenzylidene)-4-(*n*-butyl)aniline (MBBA) as an example, because its properties are well known: From Eq. (7) it follows that the correlation length $\xi_0 \approx 0.4$ nm is only a few molecular lengths. This bears two consequences: first, for the underlying mesoscopic theory to be valid, one volume element has to be large enough to contain sufficiently many molecules so that statistical mean values can be defined. Thus, all statements which refer to lengths smaller than $\approx 10\xi_0$ are not applicable to MBBA and other thermotropic nematics. Second, high resolution experiments would be needed to detect such small structures. For polymer-constituent nematics, however, and for some lyotropics, the predicted effects should be well observable.

B. Capillary

More than 20 years ago, Cladis and Kléman compared a planar $s = 1$ disclination to the escaped solution. They found the latter to be energetically preferred only for sufficiently large capillaries [13]. Later, theoretical and experimental evidence for an additional symmetry-breaking solution was reported [11]. Thus, our calculations are in agreement with previous considerations. As a result, we predict a first order symmetry-breaking configuration transition between both solutions. A phase diagram specifies under which conditions either of the two configurations should occur.

C. Droplet

In director field calculations, homeotropic droplets have usually been assumed to possess spherically symmetric director configurations when external fields are absent and rigid anchoring applies [14,15]. Using the alignment tensor formalism, Penzenstadler and Trebin have already considered a cylindrically symmetric solution [16]. We could show that this symmetry-breaking solution will be encountered ordinarily. Only for very small droplets, or very close to the nematic-isotropic phase transition, should a spherically symmetric solution occur.

ACKNOWLEDGMENTS

We thank Professor Dr. W. Muschik for valuable discussions. We are particularly grateful to Dr. M. Hinze, mathematics department, TU Berlin, for advice on the numerical techniques. This work was supported by the Deutsche Forschungsgemeinschaft via the SFB 335 "Anisotrope Fluide."

[1] P. G. De Gennes, *The Physics of Liquid Crystals* (Clarendon Press, Oxford, 1974).
[2] S. Hess, Z. Naturforsch. **30a**, 728 (1975); **30a**, 1224 (1975).
[3] N. Schopohl and T. J. Sluckin, Phys. Rev. Lett. **59**, 2582 (1987).
[4] P. Palffy-Muhoray, E. C. Gartland, and J. R. Kelly, Liq. Cryst. **16**, 713 (1994).
[5] A. Kilian, Liq. Cryst. **14**, 1189 (1993).
[6] S. Hess and I. Pardowitz, Z. Naturforsch. **36a**, 554 (1981).
[7] P. Kaiser, W. Wiese, and S. Hess, J. Non-Equilib. Thermodyn. **17**, 153 (1992).
[8] A. Sonnet, Report at the Fachbereich Mathematik, TU Berlin, 1994 (unpublished).
[9] P. Spellucci, *Numerische Verfahren der Nichtlinearen Optimierung* (Birkhäuser, Basel, 1993).
[10] G. D. Smith, *Numerical Solution of Partial Differential Equations: Finite Difference Methods*, 3rd ed. (Clarendon Press, Oxford, 1985).
[11] D. W. Allender, G. P. Crawford, and J. W. Doane, Phys. Rev. Lett. **67**, 1442 (1991).
[12] A. Sonnet, Report at the Inst. of Theoretical Physics, TU Berlin, 1992 (unpublished).
[13] P. E. Cladis and M. Kléman, J. Phys. (Paris) **33**, 591 (1972).
[14] J. W. Doane *et al.*, Mol. Cryst. Liq. Cryst. **165**, 511 (1988).
[15] N. Schopohl and T. J. Sluckin, J. Phys. France **49**, 1097 (1988).
[16] E. Penzenstadler and H.-R. Trebin, J. Phys. France **50**, 1025 (1989).